Space-time Characteristics and Experimental Analysis of Broadening First-order Sea Clutter in HF Hybrid Sky-surface Wave Radar

Yajun LI, Yinsheng WEI, Rongqing XU, Tianqi CHU, Zhuoqun WANG

School of Electronics and Information Engineering, Harbin Institute of Technology, Harbin, 150001, China

liyajun1985happy@163.com, weiys@hit.edu.cn, xurongqing@hit.edu.cn, ctqhit@126.com, wangzhuoqun_HIT@126.com

Abstract. *In high frequency (HF) hybrid sky-surface wave radar, the first-order sea clutter broadening is very complex and serious under the influence of ionosphere and bistatic angle, which affects the detection of ship target. This paper analyzes the space-time characteristics based on the HF sky-surface wave experimental system. We first introduce the basic structure, working principle and position principle based on our experimental system. Also analyzed is the influence of ionosphere and bistatic angle on the space-time coupling characteristics of broadening first-order sea clutter and the performance of space-time adaptive processing (STAP). Finally, the results of theoretic analysis are examined with the experimental data. Simulation results show that the results of experiment consist with that of theoretic analysis.*

Keywords

Space-time characteristics of first-order sea clutter, bistatic angle, ionosphere, STAP, HF hybrid sky-surface wave radar.

1. Introduction

HF sky-wave or surface-wave radar has some natural advantages, such as the capability of detecting low-flying target and stealth target, avoiding the attack of anti-radiation missile, as well as providing wide area surveillance with longer early warning time than some normal HF radar. Therefore, HF radar plays a more and more important role in modern air defense system and has potential significant contribution to military applications. Based on the propagation mode associated with HF sky-surface wave, HF hybrid sky-surface wave system is one new detection technique, which attains the information of the target and ocean surface. This technique can improve target Over-The-Horizon (OTH) detection and ocean surface dynamical environment surveillance capability. Because of the special working system and the influence of bistatic system layout, its sea echo spectrum property is more complicated than that of merely sky-wave reflection or ground-wave diffraction mode. Due to the combined influences of ionosphere and bistatic angle, the broadening of first-order sea clutter spectrum is very serious, which seriously affects the effective detection of slowly moving targets like ships.

The sea clutter spectrum is mainly composed of first-order scatter and the second-order scatter which is a continuum spectrum with amplitude less than the first-order returns about 20-45 dB. In general, the first-order returns can be denoted by two distinct Bragg lines. The first-order sea clutter characteristics of HF hybrid sky-surface wave radar are not only related to oceanic dynamics, beam width and operating frequency, but also influenced by bistatic angle and ionosphere. The time-varying characteristic and hierarchical structure of the ionosphere will cause the sea clutter Doppler frequency shift and broadening. Thus the sea clutter characteristics in the radar largely depend on the ionospheric state. In addition, the HF hybrid sky-surface wave radar is actually a bistatic radar system. Harbin Institute of Technology carried out an integrated HF sky-surface wave experimental system, but the scale of receiving arrays is so limited that the width of the received beam is quite broad, and in this condition, the bistatic angle might cause different broadening characteristics in the different resolution cells. What's worse, ionospheric contamination further contributes to the broadening characteristic of sea clutter.

P. A. Melyanovski et al. mentioned this new concept radar in 1997 [1]. G. J. Frazer described an experimental multi-static HF radar in 2007 [2]. R. J. Riddolls respectively discussed theories of the experimental configuration and the influence of ionosphere in this radar system in 2007 and 2008 [3], [4]. Jiao et al. investigated the possible application of the new mode in 2007 [5]. Jiang et al. analyzed the phenomenon in this radar system that the first-order sea clutter varies with azimuth in 2011 [6]. Lou et al. studied the frequency selection problem in 2011 [7]. Zhao et al. analyzed the detection performance of hybrid sky-surface wave propagation mode based on DRM digital AM broadcasting in 2013 [8]. Harbin Institute of Technology analyzed the detection principle and the characteristics of sea clutter by experimental system in recent years [6], [9]. However, experimental results show that

broadening of some sea clutter is serious, and difficult to effectively detect. Therefore, it requires deep study on the space-time characteristic of sea clutter in order to effectively suppress the broadening sea clutter and detect the ship target.

The paper conducts study on the space-time characteristics of first-order sea clutter in HF hybrid sky-surface wave radar. Firstly, the basic structure, working principle, radar equation and positioning principle of HF sky-surface wave experimental system were introduced respectively in Section 2. Secondly, this paper conducts detailed study on space-time characteristics of sea clutter in HF hybrid sky-surface wave radar in Section 3, and the space-time distribution and spreading model of first-order sea clutter under the action of bistatic angle and ionosphere were given. Then, space-time characteristics of sea clutter were analyzed through the simulation in Section 4, the experimental data for the space-time spreading spectrum of sea clutter in real HF sky-surface wave system were given, which verified the results of theoretical analysis. The theoretical analysis of space-time distribution for spreading sea clutter was also in agreement with experimental results. Finally, the influence of ionospheric disturbance on the performance of STAP algorithm was analyzed based on experimental data. It has been proved that serious ionospheric disturbance will influence the space-time coupling characteristics of first-order sea clutter, and lead to performance reduction of STAP. The results are useful for practical application of STAP in HF hybrid sky-surface wave radar.

2. Summarization of HF Hybrid Sky-surface Wave Experimental System

2.1 Basic Structure and Working Principle

The system layout for the HF hybrid sky-surface wave radar is shown in Fig. 1. In the HF sky-surface wave radar, skywave radar station behind the coast is used as
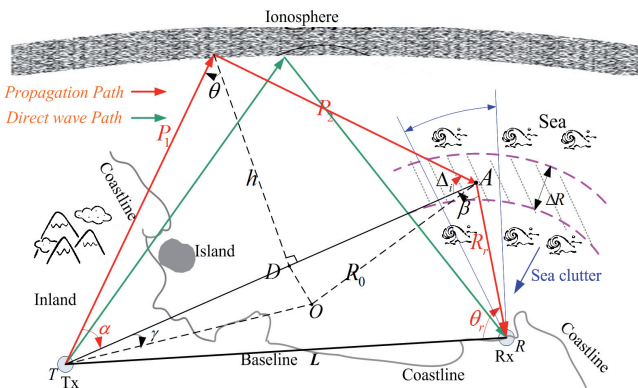

Fig. 1. The layout of HF sky-surface wave experimental system.

transmitting station, and the energy radiated by the transmitting station is reflected by ionosphere to monitor the sea

area. Then the scattering energy of sea wave and target in the monitoring sea area arrives at the ground-wave radar receiving station by ground-wave diffraction on the sea surface. Thus it realizes the acquisition of sea information and the detection of targets on the sea. In Fig. 1, L is the baseline distance between transmitting and receiving stations, R_r is the distance between target and receiving station, θ_r is the angle between R_r and baseline, h is the ionospheric reflection height, D is the distance between transmitting station and target, R_0 is the earth radius, α is the elevation angle of the emitted electromagnetic wave, θ is the reflected angle of ionosphere.

2.2 Positioning Principle

Combined with the geometric relationships in Fig. 1, the following two relationships can be obtained by the law of cosines:

$$P_1^2 = h^2 + (D/2)^2 \ , \tag{1}$$

$$D^2 = L^2 + R_r^2 - 2LR_r \cos\theta_r \ . \tag{2}$$

Distance R is obtained by the conventional time delay estimation. Fig. 1 shows that $R = P_1 + P_2 + R_r$. Assuming the ionosphere is not inclined, i.e., $P_1 = P_2$. Then, we can obtain the following formula:

$$P_1 = (R - R_r)/2 \ . \tag{3}$$

Considering equations (1) to (3), the positioning relationship of the radar system can be obtained as follows:

$$R_r = \frac{R^2 - 4h^2 - L^2}{2(R - L\cos\theta_r)} \ . \tag{4}$$

According to (4), in order to realize the target location, namely measure the distance from target to receiving station, details need to be known including the distance obtained from time-delay ranging, the azimuth of target, the ionospheric height and baseline length.

3. Analysis of Space-time Characteristics of the First-order Sea Clutter in HF Hybrid Sky-surface Wave Radar

3.1 The Space-time Characteristics of the First-order Sea Clutter with Bistatic Angle

HF radar sea clutter consists of the first, second and higher order components, of which the first-order sea clutter consists of two symmetrical peaks, namely the negative and positive first-order Bragg peaks. Its mechanism can be explained by the Bragg resonant scattering process [10]. The interaction of incident radio waves and sea waves can cause the radio wave scattering. Because the scattering

echo is caused by the first effect of HF radio waves and sea waves, this process is called the first-order effect of HF radio waves and sea waves. When the wavelength of radio and sea wave satisfies the Bragg resonance condition, Bragg resonant scattering occurs.

The Bragg frequency of first-order sea clutter in HF bistatic radar can be calculated by the following formula [10-12]:
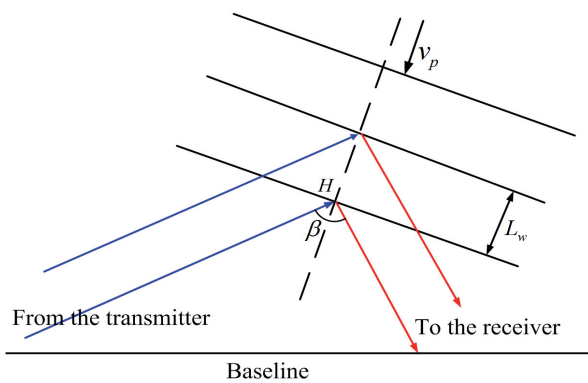
$$f_B = \pm \sqrt{\frac{gf_0}{\pi c}} \sqrt{\cos(\beta/2)} \qquad (5)$$

where f_0 is radar operating frequency, β is the bistatic angle.
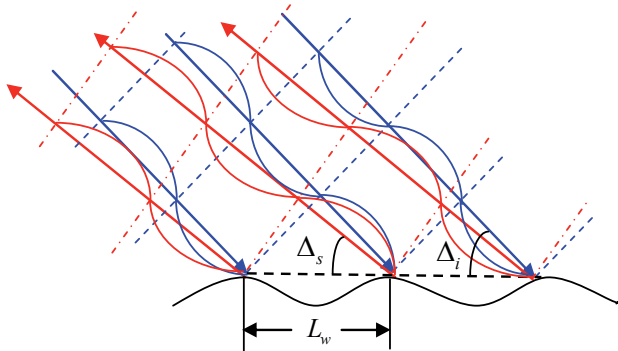
In (5), the positive and negative sign corresponds to toward and away from the radar. In fact, the Bragg resonance condition of bistatic radar is shown in Fig. 2.

$$L_w(\cos \Delta_i + \cos \Delta_s)\cos(\beta/2) = m\lambda \qquad m = 1,2,3,\ldots \quad (6)$$

where λ is radio wavelength, Δ_i is incident grazing angle, Δ_s is the angle of reflection of radio waves, L_w is sea wave length.

(a) Azimuthal plane.

(b) Elevation-angle plane.

Fig. 2. The Bragg scattering geometry of bistatic radar: (a) azimuthal plane and (b) elevation-angle plane.

When $m = 1$, corresponding to the first-order sea clutter. Considering the hybrid system radar's geometrical relation and configuration, we have the incident angle $\Delta_i = \alpha$ and the reflection angle $\Delta_s = 0$. Thus we can get the resonance condition of the first-order sea clutter under the configuration of hybrid propagation mode:

$$L = \frac{\lambda}{\cos(\beta/2)(\cos\alpha+1)} \quad . \qquad (7)$$

Waves with other wavelength will not produce coherent scattering, which echoes can be ignored. In the spectrum, the Doppler frequency shift caused by the moving velocity is:

$$f_B = \pm v_p \cos(\beta/2)(\cos\alpha+1)/\lambda \qquad (8)$$

where v_p is the moving velocity of the sea wave's phase.

Known from the theory of hydraulics, for gravity wave, its v_p and its wavelength has the following relation [12]:

$$v_p = \sqrt{gL/2\pi} \quad . \qquad (9)$$

Thus we can derive the formula of first-order sea clutter Bragg frequency of hybrid system HF OTH radar:

$$f_B = \pm \sqrt{\frac{gf_0}{\pi c}} \sqrt{\cos(\beta/2)} \sqrt{\frac{\cos\alpha+1}{2}} \quad . \qquad (10)$$

The bistatic angle β can be obtained by geometric relation in Fig. 1:

$$R_t^2 = R_r^2 + L^2 - 2R_r L \cos\theta_r \quad , \qquad (11)$$

$$L^2 = R_t^2 + R_r^2 - 2R_r R_t \cos\beta . \qquad (12)$$

Combining with (10)-(12), we can derive the space-time distribution of first-order sea clutter with angle-Doppler in HF hybrid sky-surface wave radar:

$$f_B = \pm \sqrt{\frac{gf}{\pi c}} \sqrt{\frac{\cos\alpha+1}{2}}$$
$$\cdot \sqrt{\frac{1}{2} + \frac{R_r - L\cos\theta_r}{2\sqrt{R_r^2 + L^2 - 2R_r L\cos\theta_r}}} \qquad (13)$$

From the above formula (13), we can see the Bragg frequency of first-order sea clutter in HF hybrid sky-surface wave is a function of the bistatic angle, range cell, and also the radar looking direction. In distance R_r, the Bragg frequency f_B of first-order sea clutter varies with azimuth angle θ_r (the angle between beam pointing and baseline) changes, and shows the obvious angle-Doppler coupling characteristics.

Next, we need to analyze the spreading range of the first-order Bragg frequency for the HF hybrid propagation mode. Harbin Institute of Technology developed an integrated HF sky-surface wave radar experimental system in recent years. Given the size and cost of this radar system, the array aperture of the receiving array for our experimental system is small. Thus the width of the received beam is quite broad, the scattering cell E corresponding to a certain range gate cannot be equivalent to a point but a small area, leading to the corresponding bistatic angle is not a single value β, but a range of $\beta \in [\beta_{min}, \beta_{max}]$. Therefore, the

Bragg frequency of first-order sea clutter is also a range of $f_B \in \left[f_{B_{min}}, f_{B_{max}} \right]$. Thus, the theoretical broadening value Δf_B caused by bistatic angle is calculated by (14):

$$\Delta f_B = f_{B_{max}} - f_{B_{min}}$$
$$= \sqrt{\frac{g}{\pi \lambda}} \left(\sqrt{\cos \left(\frac{\beta_{min}}{2} \right)} - \sqrt{\cos \left(\frac{\beta_{max}}{2} \right)} \right) . \quad (14)$$

3.2 The Space-time Characteristics of First-order Sea Clutter with Ionosphere Disturbance

HF sky-surface wave radar echo is also influenced by the ionospheric disturbance. Ionospheric phase path approximately moves with the variable motion for a long CIT, and the phase path variation of radio wave is also nonlinear variation, resulting in sea clutter spectral broadening [14]-[17]. In this paper, two typical ionosphere contamination functions (corresponding to two different ionospheric motion state) are used to simulate the space-time spectrum of contaminated sea clutter with ionospheric disturbance: (1) sine phase contamination mode: $\phi_1(t) = A_m \sin(\omega_m t)$, and (2) polynomial phase contamination mode: $\phi_2(t) = 2\pi \left(a_0 + a_1 t + a_2 t^2 \right)$.

The space-time distribution of first-order sea clutter under the action of bistatic angle and ionospheric disturbance for HF hybrid sky-surface wave radar can be expressed as:

$$f_B = \sqrt{\frac{g}{\pi \lambda} \cdot \frac{\cos \alpha + 1}{2}} \cdot \sqrt{\sqrt{\frac{1}{2} + \frac{R_r - L \cos(\theta_i)}{2 \sqrt{R_r^2 + L^2 - 2 R_r L \cos \theta_i}}}}$$

$$+ \frac{1}{2\pi} \frac{d(\phi_i(t))}{dt}$$

$$\quad (15)$$

$$= \pm 0.102 \times 10^{-3} \sqrt{f_0(MHz) \cdot \frac{\cos \alpha + 1}{2}}$$

$$\cdot \sqrt{\sqrt{\frac{1}{2} + \frac{R_r - L \cos(\theta_i)}{2 \sqrt{R_r^2 + L^2 - 2 R_r L \cos \theta_i}}} + \frac{1}{2\pi} \frac{d(\phi_i(t))}{dt}}$$

Ionospheric disturbance also cause first-order sea clutter spectrum broadening. Here

$$\Delta f_B = \left[\max \left(d(\phi_i(t)) / dt \right) - \min \left(d(\phi_i(t)) / dt \right) \right] / 2\pi$$

is used to represent the sea clutter broadening caused by ionosphere. Combining with (14), we can derive and obtain the biggest possible broadening value Δf_B of first-order sea clutter Bragg frequency under the action of bistatic angle and ionospheric disturbance:

$$\left[-0.102 \times 10^{-3} \sqrt{f_0(MHz) \cdot \cos \left(\frac{\beta_{min}}{2} \right)} + f_{ion\_min}, \right.$$

$$\left. -0.102 \times 10^{-3} \sqrt{f_0(MHz) \cdot \cos \left(\frac{\beta_{max}}{2} \right)} + f_{ion\_max} \right] \quad (16)$$

$$\left[+0.102 \times 10^{-3} \sqrt{f_0(MHz) \cdot \cos \left(\frac{\beta_{max}}{2} \right)} + f_{ion\_min}, \right.$$

$$\quad (17)$$

$$\left. +0.102 \times 10^{-3} \sqrt{f_0(MHz) \cdot \cos \left(\frac{\beta_{min}}{2} \right)} + f_{ion\_max} \right]$$

where f_{ion_min} and f_{ion_max} represent the maximum and minimum instantaneous frequency caused by ionosphere, respectively.

The following uses the formula (16) and (17) to quantitatively represent the degree of sea clutter broadening. Here f_{dbin} represents the Doppler resolution cell.

$$\varepsilon = \frac{\Delta f_B}{f_{dbin}} . \quad (18)$$

The sea clutter signal within range cell l can be expressed by the superposition of K scatter point return signals with each angle-range resolution cell. Therefore, the broadening sea clutter signal model with combined actions of bistatic angle and ionosphere can be written as the following form:

$$s(t) = \sum_{i=1}^{K} a_i(t) \cdot \left[\exp(j 2\pi f_B t) + \exp(-j 2\pi f_B t) \right]$$
$$\cdot \exp(j \phi_i(t)) \quad (19)$$

where $a_i(t)$ is the amplitude of signal component, meets Gaussian distribution; $f_B (i = 1 \ldots K)$ is K complex frequency component within Bragg frequency band, and $f_{B\_min} \le f_B \le f_{B\_max}$; $\phi_i(t)$ is the ionospheric phase contamination function.

3.3 Analysis of Space-time Coupling Characteristics of the First-order Sea Clutter

The bistatic angle characteristics of HF hybrid sky-surface wave radar make the first-order sea clutter has obvious space-time coupling characteristics. In order to quantitatively analyze the influence of ionosphere contamination on space-time coupling characteristics of sea clutter, this paper defines the average derivative ξ. Assume that positive and negative Bragg peak is affected by the ionospheric disturbance, ξ is defined as the mean of Doppler frequency derivative on the sine of angle. Here, the above Doppler frequency refers to the Doppler frequency at the position of the power of positive Bragg peak at each beam pointing within range cell l (Nth beam pointing).

$$\xi_l = \frac{1}{N} \sum_{i=1}^{N} \frac{d\left(f_{B_{\theta_i,max}} \right)}{d\left(\sin \theta_i \right)} . \quad (20)$$

Doppler frequency of ground clutter has a linear relation with the sine of angle for airborne side-looking radar, therefore $\xi = 1$, which has strong space-time coupling. The Doppler frequency of first-order sea clutter is constant

value and independent of angle in HF surface wave radar (HFSWR), therefore $\xi \to 0$, which almost do not have the space-time coupling (the coupling relationship between angle and Doppler). From (13), we know that the Doppler frequency of first-order sea clutter changes with angles for HF hybrid sky-surface wave radar, and its space-time coupling characteristics are between airborne radar and HFSWR, and the space-time distribution is relatively smooth, so using the defined average derivative ξ in this paper can better analyze the space-time coupling characteristics.

4. Simulation and Experimental Analysis of Space-time Distribution of First-order Sea Clutter

4.1 The Space-time Distribution of First-order Sea Clutter with Bistatic Angle

Fig. 3 shows the array layout diagram of HF sky-surface wave experimental system. System parameters: baseline length $TR = L = 800$ km; normal direction is 50° counterclockwise from north; operating frequency $f_0 = 10$ MHz; uniform linear receiving array element $N = 8$, array element spacing $d = 20$ m; digital beam forming (DBF) DBF =-30°-30°, CIT = 40 s.
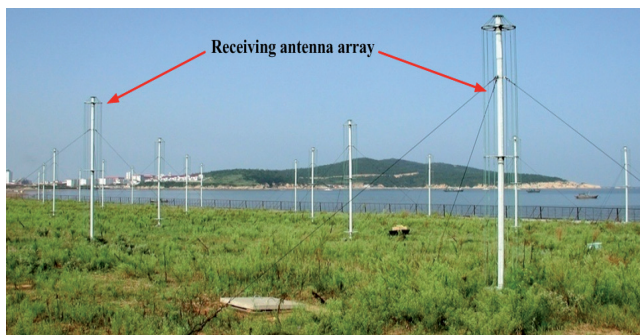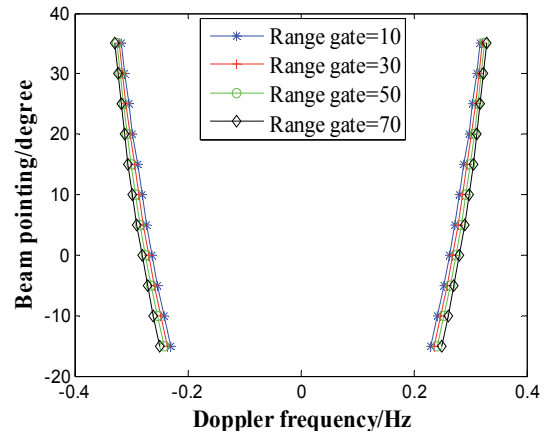

(a) Actual receiving antenna array of HF sky-surface wave system.
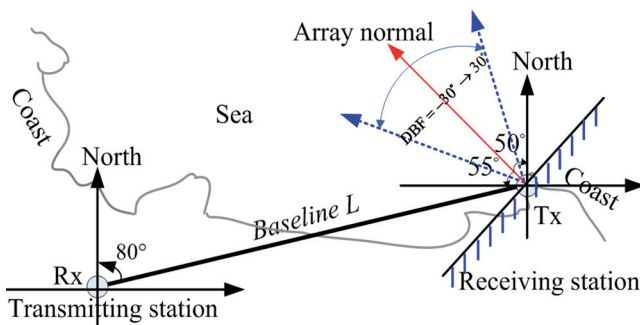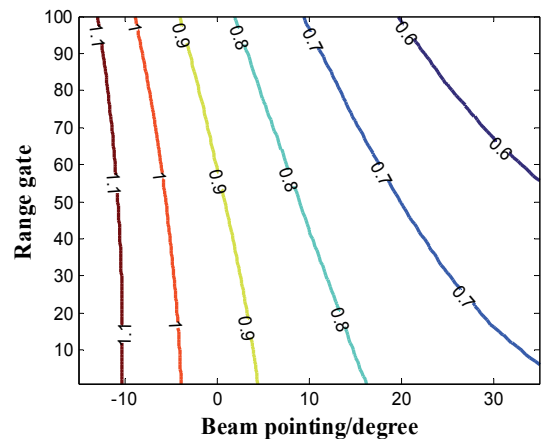

(b) Array geometric diagram of the transmitting station and the receiving station.

Fig. 3. Array layout diagram of HF sky-surface wave radar.

(a) Theoretical space-time distribution of sea clutter.

(b) Theoretical broadening characteristics of sea clutter.

Fig. 4. The theoretical distribution characteristics of first-order sea clutter spectrum without the influence of ionosphere.

The space-time distribution characteristics of first-order sea clutter with different ranges are simulated and analyzed. It is noted that there is no consider the effect of the ionosphere. From Fig. 4(a), we can see that it is consistent with the space-time distribution characteristics of first-order sea clutter at different range cells. For the same azimuth angle, the corresponding bistatic angle decreases and Doppler frequency increases with range increasing, so there are Doppler frequency shifts between range cells. From (15), we can see that the Doppler frequency of first-order sea clutter increases with the increase of the azimuth angle at the same range cell, showing the obvious space-time coupling characteristics.

According to (16) and (17), calculate and simulate the broadening characteristics of first-order sea clutter. Here, formula (18) is used as the sea clutter broadening measurement. Fig. 4(b) shows the theoretical broadening characteristics (unit: Hz) of the first-order sea clutter Bragg frequency with different ranges and azimuths. From Fig. 4(b), we can see that: (1) when the azimuth angle θ_r is little, corresponding to large bistatic angle, sea clutter broadening is serious within some receiving beam width; (2) when the azimuth angle θ_r increases, the broadening extent is small which is similar to the monostatic HFSWR.

4.2 The Space-time Distribution of First-order Sea Clutter with Ionospheric Disturbance

Combining with (19) and different ionospheric phase contamination functions, the space-time distribution of first-order sea clutter with angle-Doppler at range gate = 30 was simulated and analyzed, as shown in Fig. 5. The black line represents the theoretical space-time distribution of first-order sea clutter without the influence of ionosphere. Compared with the characteristics of HF bistatic radar, sine contamination function of ionospheric phase path makes the space-time spectrum broadening obviously, polynomial contamination function of ionospheric phase path makes the space-time spectrum produced obvious Doppler frequency shift and broadening.
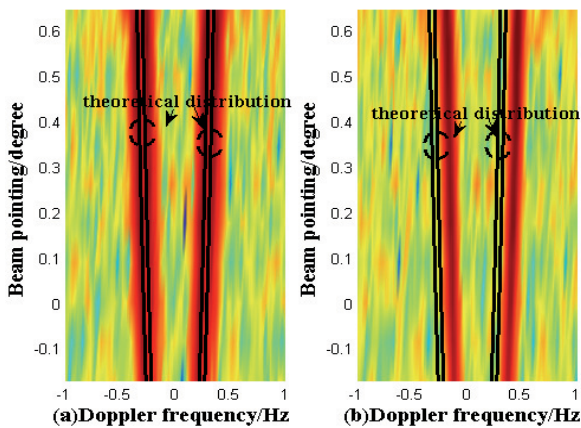

Fig. 5. The space-time distribution characteristics of first-order sea clutter with the influence of ionosphere: (a) space-time distribution of sea clutter with sine phase contamination mode; (b) space-time distribution of sea clutter with polynomial phase contamination mode.

4.3 Analysis of Space-time Coupling Characteristics of First-order Sea Clutter with Ionospheric Disturbance

Combining with the previous analysis, the influence of the Doppler frequency shift and broadening caused by ionospheric disturbance on space-time coupling of first-order sea clutter was analyzed. The ionospheric phase contamination function is set to [17]:

$$\phi(t) = \omega_{m0} t + A_m \sin(\omega_m t) \qquad (21)$$

where, ω_{m0} is the translation frequency, A_m and ω_m is respectively the amplitude and frequency of periodic item. $A_m \sin(\omega_m t)$ was used to control the degree of sea clutter broadening caused by ionosphere; ω_{m0} was used to control the degree of the Doppler frequency shift of sea clutter. From Fig. 6(a), we can see that sea clutter has a certain space-time coupling characteristics under the array configuration, $\xi \approx 0.1$. When there is not Doppler frequency shift disturbance ω_{m0} between beam forming, single Dop-

pler spectrum broadening $A_m \sin(\omega_m t)$ will not cause serious influence on space-time coupling of first-order sea clutter, approaching the ideal first-order sea clutter without the influence of ionosphere. When there is Doppler frequency shift disturbance, space-time coupling characteristics of sea clutter significantly deviate from the ideal first-order sea clutter without the influence of ionosphere, and the more serious the frequency shift disturbance, the more obvious the space-time coupling characteristics of sea clutter change.

Through the simulation and analysis, we can get the same conclusion by polynomial phase contamination function. Fig. 6(b) shows the comparison of space-time coupling characteristics of ideal and measured sea clutter under different array layouts. Here, array layout 1 refers to the angle between normal direction of receiving array and baseline is 150°; array layout 2 refers to the angle is 50°. From Fig. 6(b), we can see that actual space-time coupling of sea clutter was affected by the ionosphere. The space-time coupling from ideal sea clutter without the influence of ionosphere is identical to the actuality of experimental system in array layout 1.
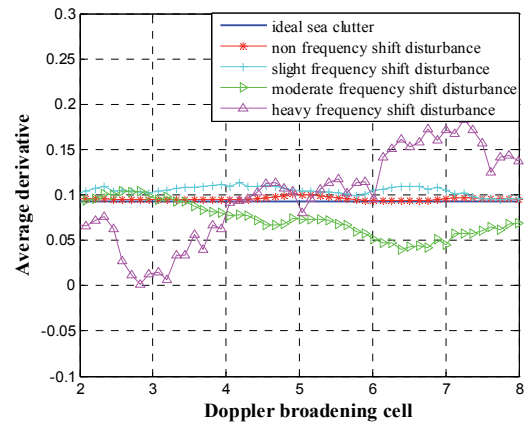
(a) Simulation of influence of ionospheric disturbance on space-time coupling characteristics of sea clutter.
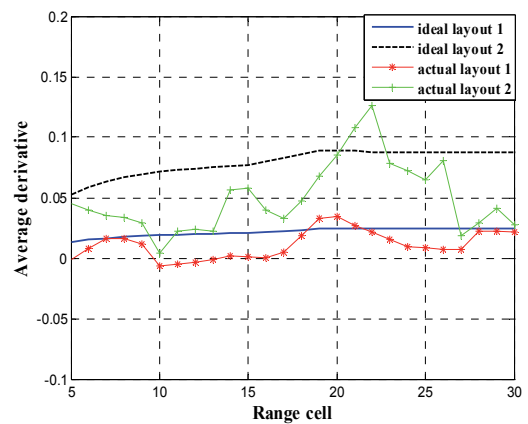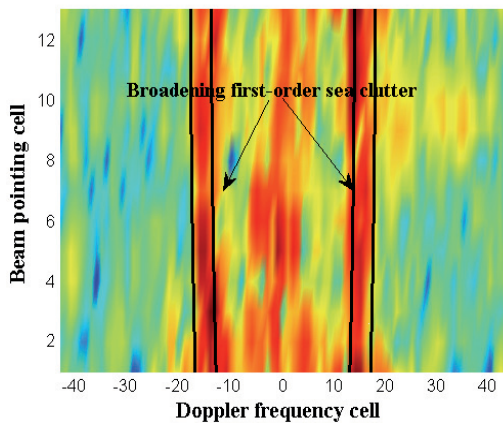

(b) Comparison of space-time coupling characteristics of ideal and measured sea clutter.

Fig. 6. Analysis of space-time coupling characteristics of first-order sea clutter.
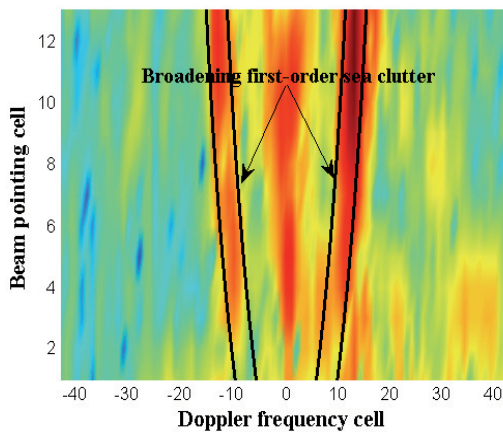
4.4 Comparative Analysis of Theoretical Simulation and Experimental Results

With the support of the developed integrated HF sky-surface wave radar experimental system, experimental data were analyzed with the theoretical simulation. System parameters: Baseline length $TR = 800$ km, operating frequency $f_0 = 13$ MHz, CIT = 43 s, receiving array element $N = 8$, array element interval $d = 20$m, repetition interval is 20 ms. The angle between normal direction of receiving array and baseline respectively is 150° (array layout 1) and 50° (array layout 2). Processing of experimental data includes pulse compression, beam forming, coherent accumulation, etc.

In Fig. 7, the black line represents the space-time distribution of first-order sea clutter under the action of bistatic angle and ionospheric phase contamination (obtained by direct wave) by (16) and (17). It is noted that the direct wave path in Fig. 1 represents that from the sky-wave station to the ionosphere and then directly reflects back to ground-wave stations, therefore, the direct echoes are only under the influence of the ionosphere, while not affected by the bistatic layout. For this reason, we can take advantage of the direct wave data to analyze the influence of ionosphere on sea clutter. As can be seen from Fig.7, the

theoretical and measured results are basically met. The angle between normal direction of receiving array and baseline of array layout 2 is much smaller than array layout 1. Therefore, the change of bistatic angle is very obvious and Bragg frequency of first-order sea clutter has obvious differences at different azimuths in array layout 2, and λ is large, space-time coupling is strong.

From Fig. 7, we can see that there is frequency shift disturbance caused by ionosphere at different ranges and azimuths in real-world environments, causing the obvious changes of space-time coupling of sea clutter between theoretical and practical, and the difference between different ranges is larger, space-time coupling characteristics of sea clutter at most of range cells is less than ideal situation.

In the following, the influence of ionospheric disturbance on sea clutter spectrum was analyzed by comparing the simulated and measured Doppler spectrum of sea clutter, as shown in Fig. 8. Through the oblique ionogram corresponding the batch of measured data at that moment [18], we know that the transmitting electromagnetic wave reflects at layer Es when $f_0 = 13$ MHz, which means no multimode effects. The mean of ideal sea clutter broadening without the influence of ionosphere at 3 dB below the two

(a) Array layout 1, range cell = 37.
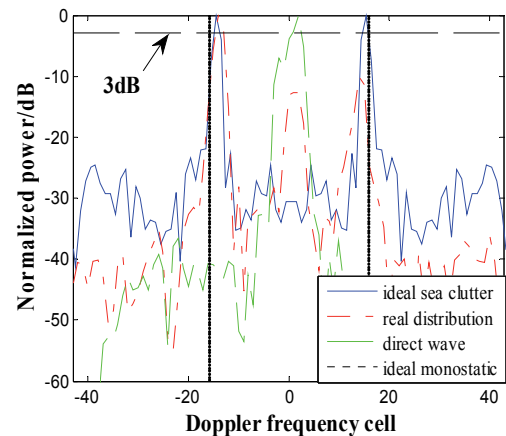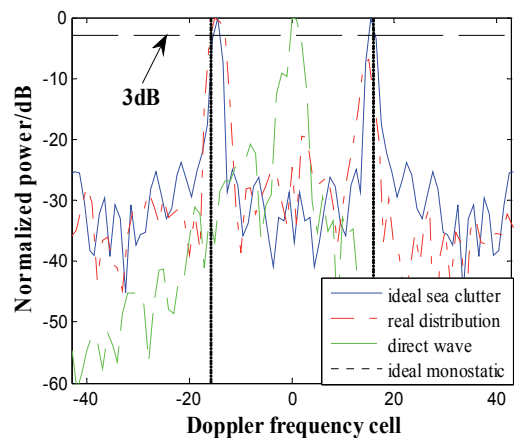

(b) Array layout 2, range cell = 8.

Fig. 7. Analysis of angle-Doppler distribution of measured first-order sea clutter.

(a) Range cell = 27, azimuth angle =-25°.

(b) Range cell = 27, azimuth angle =-15°.

Fig. 8. Comparison of ideal and measured sea clutter Doppler spectrum.

Bragg peak $(\Delta f^{+} + \Delta f^{-})/2$ is used as spectrum broadening measurement. Fig. 8 shows the Doppler spectrum of first-order sea clutter at the same range cell = 27 with two different azimuth angles. The Doppler spectrum of the real direct wave signal has significant broadening, and there is obvious broadening by comparison of ideal and measured sea clutter at different azimuths.

Tab. 1 shows the degree of Doppler broadening of first-order sea clutter at range cells = 27-30 (R27-R30) with different azimuth angles DBF = -25°-25° (interval 5°, B1-B11). From Tab. 1, we can see that there is obvious broadening at different azimuths. We can obtain the Doppler spectrum broadening of direct wave is about 0.04 Hz by the method of literature [14], which is consistent with the actual broadening value.

It should be noted that the broadening value of sea clutter at different azimuths is not identical; this is due to spatial difference of ionospheric propagation path at different azimuths. Through the analysis of measured data we find that the spatial difference of ionospheric propagation path is small.

Broadening /Hz	B1	B3	B5	B7	B9	B11
R27	0.035	0.045	0.017	0.017	0.033	0.034
R30	0.025	0.040	0.034	0.023	0.018	0.017

Tab. 1. First-order sea clutter broadening at different azimuths.

5. Influence of Ionospheric Disturbance on the Performance of STAP

STAP is a kind of low complexity and effective way for using training samples to suppress clutter, having become an important direction of research scholars from various countries and has been used in airborne radar [19]-[21]. Similar to HF ground clutter [19], [20], there are angle-Doppler coupling characteristics of sea clutter in HF hybrid sky-surface wave radar; so, using STAP to suppress broadening sea clutter becomes possible. The Joint Domain Localized (JDL) algorithm mainly takes advantage of the transformation vector **T** to transform the space-time data to the angle-Doppler domain and select a small local area for adaptive processing [19]. It is a kind of dimension reduced algorithm of the STAP processing, solving the lack of training samples and excessive computation load.

5.1 JDL Algorithm Principle

Space Time Adaptive Processing is using the training samples close to the range bin to be detected to estimate clutter and noise covariance matrix **R**, and according to linearly constrained minimum variance criteria (LCMV) to estimate adaptive weights w, and then weight the received data to maximize SNR. Covariance matrix is given by:

$$\mathbf{R} = \frac{1}{K}\sum_{i=1}^{K} \mathbf{X}_i \cdot \mathbf{X}_i^{H} \qquad (22)$$

wherein, $\mathbf{X}_i$ is a training sample data.

Weight vector can be given by:

$$\mathbf{w} = \mu\mathbf{R}^{-1}\mathbf{v} = \mu\left(\mathbf{R}^{-1/2}\right)\left(\mathbf{R}^{-1/2}\mathbf{v}\right) \qquad (23)$$

wherein, μ is a complex normalized constant.

The JDL algorithm mainly takes advantage of the transformation vector **T** to transform the space-time data to the angle-Doppler domain, and select a small local area for adaptive processing. It is a kind of dimension reduced algorithm of the STAP processing, solving the lack of training samples and excessive computation load.

S_s and S_t respectively are space steering vector and time steering vector. Elements of them are the discrete Fourier transform coefficients. Therefore, the inner product of the spatial and temporal steering vector is equivalent to 2-D DFT , and then the process of transforming the received data from space-time domain to the ith angle bin w_{si}, the jth Doppler bin we concern can be expressed as:

$$\mathbf{X} = \left(\mathbf{S_s}\left(w_{si}\right)\right)\otimes\left(\mathbf{S_t}\left(w_{tj}\right)\right)^{H}\mathbf{X} \ . \qquad (24)$$

The JDL algorithm transforming matrix can be represented as:

$$\mathbf{T} = \begin{pmatrix} \left[\mathbf{S_s}(w_{si})\otimes\mathbf{S_t}(w_{tj})\right]^{T} \\ \left[\mathbf{S_s}(w_{si})\otimes\mathbf{S_t}(w_{tj}+w_k)\right]^{T} \\ \vdots \\ \left[\mathbf{S_s}(w_{si})\otimes\mathbf{S_t}(w_{tj}+(q-1)w_k)\right]^{T} \\ \vdots \\ \left[\mathbf{S_s}(w_{si}+(p-1)w_n)\otimes\mathbf{S_t}(w_{tj}+(q-1)w_k)\right]^{T} \end{pmatrix}^{T} \qquad (25)$$

w_n and w_k respectively represent angle and Doppler interval, p represents the number of adjacent angle bins, q represents the number of adjacent Doppler bins. Schematic diagram Fig. 9 is as follows:
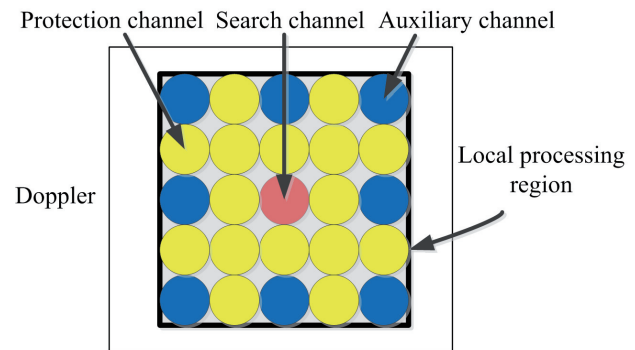

Fig. 9. JDL schematic diagram.

In Fig. 9, the red channel is the search channel, the blue channel is auxiliary channel, and the yellow channel is protection channel. The selection of a protection channel in angle-Doppler domain may be effective in preventing the spread of the target signal to clutter covariance matrix, affecting the actual detection performance.

When select the 3×3 local shown in Fig. 9, space-time transformation matrix can be expressed as:

$$\mathbf{T} = \left[\mathbf{S_t}\left(w_{t,j-2}\right); \mathbf{S_t}\left(w_{t,j}\right); \mathbf{S_t}\left(w_{t,j+2}\right) \right] \\ \otimes \left[\mathbf{S_s}\left(w_{s,i-2}\right); \mathbf{S_s}\left(w_{s,i}\right); \mathbf{S_s}\left(w_{s,i+2}\right) \right] \quad (26)$$

The transformed space-time steering vector is:

$$\tilde{\mathbf{v}} = \mathbf{T}^H \cdot \mathbf{v} \quad . \quad (27)$$

The receiving data vector is:

$$\tilde{X} = T^H \cdot X \quad . \quad (28)$$

The corresponding adaptive weight vector is:

$$\tilde{w} = \mu \tilde{R}^{-1} \tilde{v} \quad . \quad (29)$$

5.2 Experimental Results

The target is injected into the position of range cell = 50 and azimuth angle = 0° of measured data under array layout 2, signal to clutter ratio (SCR) is SCR = -5 dB. The performance of JDL algorithm with contaminated sea clutter is analyzed by measured data. Improvement factor IF is used as the performance measurement:

$$IF = \frac{SCR_{out}}{SCR_{in}} \quad . \quad (30)$$

Fig. 10(a)-(b) show the performance of JDL algorithm with ideal and contaminated point target (because of target signal is also contaminated by ionosphere in practice) based on the measured data. The ideal point target without the influence of ionospheric disturbance is analyzed in Fig. 10(a); the contaminated point target with the influence of ionospheric disturbance is analyzed in Fig. 10(b). In Fig. 10(a)-(b), the blue solid line represents the performance of JDL with contaminated sea clutter; the red dotted line represents the performance of JDL after decontamination, where phase gradient algorithm (PGA) was used to ionospheric phase decontamination.

As can be seen from Fig. 6 in Section 4.3 and Fig. 10(a)-(b): (1) space-time coupling characteristics of sea clutter is stable when there is no ionospheric disturbance; even if the Doppler spectrum of sea clutter gradually broadening and submerged target, JDL algorithm can effectively suppress the sea clutter and find target, improvement factor is above 10 dB; (2) when there is ionospheric disturbance, space-time coupling of sea clutter is significantly affected, and clutter distribution between the training sample is no longer even, the improvement factor of JDL algorithm decreased; (3) the more severe iono-
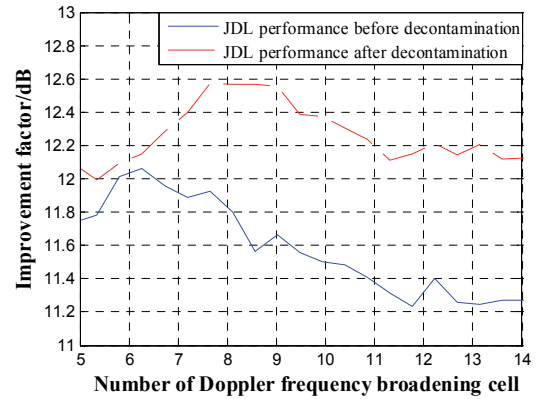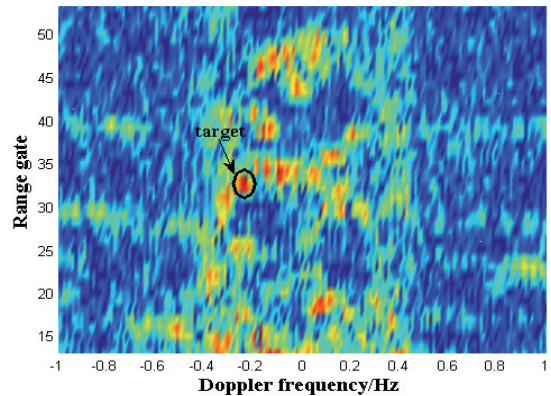

(a) Ideal point target without ionospheric disturbance is injected.
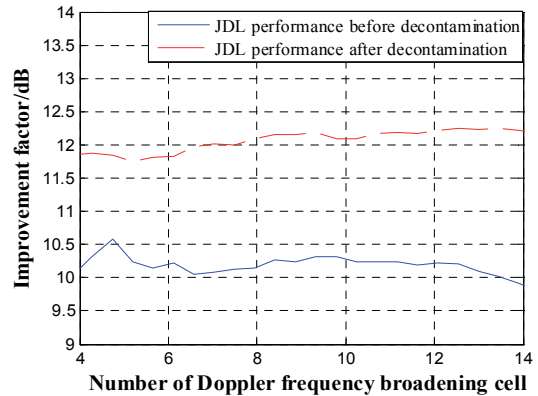
(b) Contaminated point target with ionospheric disturbance is injected.
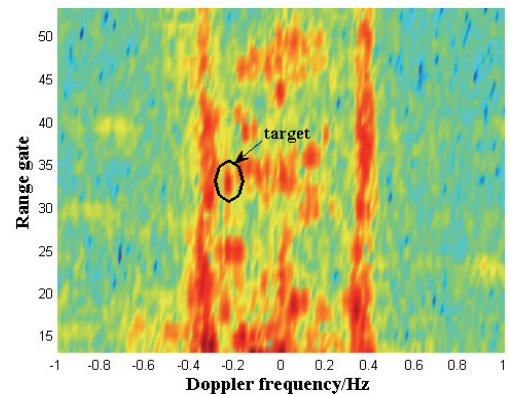
(c) Measured sea clutter spectrum with range-Doppler distribution.

(d) Measured sea clutter suppression by PGA&JDL algorithm.

Fig. 10. Analysis of performance of JDL algorithm with measured data.

spheric disturbance, the more obvious the decrease of the improvement factor; (4) the JDL performance after decontamination is superior to the JDL performance before decontamination.

Fig. 10(c)-(d) show the measured sea clutter spectrum with range-Doppler distribution (DBF = -15°) and the sea clutter suppression results after PGA&JDL algorithm. From Fig. 10(c)-(d), we can see that the measured sea clutter is significantly reduced by PGA&JDL processing, thus the PGA&JDL algorithm can achieve good suppression performance for broadening sea clutter.

6. Conclusions

In this paper, the basic working principle of HF sky-surface wave experimental system was firstly introduced. Secondly, the space-time characteristics of sea clutter were analyzed, and space-time distribution and spreading model of the first-order sea clutter under the action of bistatic angle and ionosphere were given. Then, space-time coupling characteristics of sea clutter were analyzed through the simulation, and the results of theoretical analysis were examined with the experimental results based on our developed integrated HF sky-surface wave radar system. The theoretical analysis of space-time distribution for spreading sea clutter is also in agreement with experimental results. Finally, the influence of ionospheric disturbance on the performance of STAP algorithm was analyzed based on experimental data.

It must be pointed out that these are just preliminary results and there is still a need for more studies and improvements. More details about the broadening sea clutter suppression for HF hybrid sky-surface wave radar need to be investigated to improve the detection performance. In addition, target detection and localization are also key areas of our future work.

Acknowledgements

References

[1] MELYANOVSKI, P. A., TOURGENEV, I. S. Bistatic HF radar for oceanography applications with the use of both ground and space waves. *Telecommunications and Radio Engineering*, 1997, vol. 51, no. 2, p. 73–79.

[2] FRAZER, G. J. Forward-based receiver augmentation for OTHR. In *2007 IEEE Radar Conference*. Boston (MA, USA), April 2007, p. 373–378.

[3] RIDDOLLS, R. J. Ship detection performance of a high frequency hybrid sky-surface wave radar. *Defense R&D Canada-Ottawa*, 2007, p. 1–42.

[4] RIDDOLLS, R. J. Limits on the detection of low-Doppler targets by a high frequency hybrid sky-surface wave radar system. In *IEEE Radar Conference 2008*. Rome (Italy), May 2008, p. 1–4.

[5] JIAO PEINAN, YANG LONGQUAN, FAN JUNMEI New propagation mode associating with HF sky-and-surface wave and its application. *Chinese Journal of Radio Science*, 2007, vol. 22, no. 5, p. 746–750.

[6] WEI JIANG. WEI-BO, D., QIANG, Y. Analyses of sea clutter for HF over the horizon hybrid sky-surface wave radar. *Journal of Electronic & Information Technology*, 2011, vol. 33, no. 8, p. 1786–1791.

[7] LOU PENG, FAN JUNMEI, JIAO PEINAN, YANG LONG-QUAN The operating frequency selection in HF hybrid sky-surface wave radar. In *9th International Symposium on Antennas, Propagation and EM Theory (ISAPE)*. 2010, p. 513–516.

[8] ZHIXIN ZHAO, XIANRONG WAN, DELEI ZHANG, FENG CHENG An experimental study of HF passive bistatic radar via hybrid sky-surface wave mode. *IEEE Transactions on Antennas and Propagation*, 2013, vol. 61, no. 1, p. 415-424.

[9] YAJUN LI, YINSHENG WEI Analysis of first-order sea clutter spectrum characteristics for HF sky-surface wave radar. In *2013 International Conference on Radar*. Adelaide (Australia), 9-12 September 2013, p. 368–373.

[10] TRIZNA, D., GORDON, J. Results of a bistatic HF radar surface wave sea scatter experiment. In *IEEE International Geoscience and Remote Sensing Symposium*. 2002, vol. 3, p. 1902–1904.

[11] BARRICK, D. Remote sensing of sea state by radar. In *IEEE International Conference on Engineering in the Ocean Environment*. 1972, p. 186–192.

[12] GILL, E. The scattering of high frequency electromagnetic radiation from the ocean surface: An analysis based on a bistatic ground wave radar configuration. *PhD Thesis*. Faculty of Engineering and Applied Science, Memorial University of Newfoundland, 1999, p. 1–178.

[13] WALSH, J., HUANG, W., GILL, E. The first-order HF radar ocean surface cross section for an antenna on a floating platform. *IEEE Transactions on Antennas and Propagation*, 2010, vol. 58, p. 2994–3003.

[14] GEORGES, T. M. The effects of space and time resolution on the quality of sea echo Doppler spectra measured with HF sky wave radar. *Radio Science*, 1979, vol. 14, p. 455–469.

[15] DAVIES, K., BARKER, D. M. On frequency variations of ionospherically propagated HF radio signals. *Radio Science*, 1966, p. 545–556.

[16] BOURDILLON, A., GAUTHIER, F., PARENT, J. Use of maximum entropy spectral analysis to improve ship detection by over-the horizon radar. *Radio Science*, 1987, vol. 22, no. 2, p. 313–320.

[17] PARENT, J., BOURDILLON, A. A method to correct HF skywave ionosphere frequency modulation. *IEEE Transactions on Antennas and Propagation*, 1988, vol. 36, no. 1, p. 127–135.

[18] REINISH, B. W. Ionospheric sounding in support of over-the-horizon radar. *Radio Science*, 1997, vol. 32, no. 4, p. 1689–1694.

[19] SALEH, O., ADVE, R. S., RIDDOLLS, R. J., RAVAN, M., PLATANIOTIS, K. Adaptive processing in high frequency surface wave radar. In *Proceeding of the IEEE Radar Conference, RADAR 2008*. Rome (Italy), 2008, p. 1–6.

[20] RAVAN, M., ADVE, R. S. Robust STAP for HFSWR in dense target scenarios with nonhomogeneous clutter. In *2012 IEEE Radar Conference*. Atlanta (GA, USA), May 2012, p. 0028–0033.

[21] FABRIZIO, G. A., FRAZER, G. J., TURLEY, M. D. STAP for clutter and interference cancellation in a HF radar system. In *2006 IEEE International Conference on Acoustics, Speech and Signal Processing*. Toulouse (France), vol. 4, p. 14–19.

About Authors ...

Yajun LI was born in 1983. He received the M.S. degree in Information and Communication Engineering from Harbin Engineering University in 2011. He is now a PhD student of the School of Electronics and Information Engineering at Harbin Institute of Technology, China. His current research interests include space-time adaptive processing, suppression of sea clutter, and HF radar system simulation.

Yinsheng WEI was born in 1974. He received his M.S. and Ph.D. degrees in Communication and Information Systems from Harbin Institute of Technology (HIT) in 1998 and 2002, respectively. And then, he joined the Department of Electronics Engineering in HIT as a lecturer, and became a professor in 2011. He is a member of IEEE AES, and a senior member of CIE. His main researches include radar signal processing and radar system analysis and simulation.

Rongqing XU was born in 1958. He received his M.S. and Ph.D. degrees in Communication and Information Systems from Harbin Institute of Technology (HIT) in 1984 and 1990, respectively. He is a professor at the Department of Electronics Engineering in HIT. His research interests are in the fields of radar signal processing, multi-target tracking and data processing.

Tianqi CHU was born in Heilongjiang, China, in 1989. He received the B.S. degree in Electronic Information Engineering from Harbin Institute of Technology in 2012. He is currently proceeding the M.S. degree in Electronics and Communication Engineering in HIT. His researches mainly focus on electromagnetic waves transmission and signal processing in HF OTH radar.

Zhuoqun WANG was born in 1985. She received the M.S. degree in Information and Communication Engineering from Harbin Engineering University in 2011. She is now a PhD student of the School of Electronics and Information Engineering at Harbin Institute of Technology, Harbin, China. Her current research interests include SAR imaging processing and radar signal processing.